

Discovery of an Exceptional Optical Nebulosity in the Suspected Galactic SN Iax Remnant Pa 30 Linked to the Historical Guest Star of 1181 CE

ROBERT A. FESEN,¹ BRADLEY E. SCHAEFER,² AND DANA PATCHICK³

¹6127 Wilder Lab, Department of Physics and Astronomy, Dartmouth College, Hanover, New Hampshire, 03755, USA

²Department of Physics and Astronomy, Louisiana State University, Baton Rouge, Louisiana, 70820, USA

³Deep Sky Hunters Consortium, Los Angeles, California, 90025, USA

ABSTRACT

A newly recognized young Galactic SN remnant, Pa 30 (G123.1+4.6), centered on a hot central star with a $\sim 16,000 \text{ km s}^{-1}$ wind velocity has recently been proposed to be the result of a double-degenerate merger leading to a SN Iax event associated with the guest star of 1181 CE. Here we present deep optical [S II] $\lambda\lambda 6716, 6731$ images of Pa 30 which reveal an extraordinary and highly structured nebula $170''$ in diameter with dozens of long ($5'' - 20''$) radially aligned filaments with a convergence point near the hot central star. Optical spectra of filaments indicate a peak expansion velocity $\simeq 1100 \text{ km s}^{-1}$ with electron densities of ≤ 100 to 700 cm^{-3} , and a thick shell-like structure resembling its appearance in $22 \mu\text{m}$ WISE images. No H α emission was seen ([S II] $\lambda 6716/\text{H}\alpha > 5$), with the only other line emission detected being faint [Ar III] $\lambda 7136$ suggesting a S, Ar-rich but H-poor remnant. The nebula's angular size, estimated 2.3 kpc distance, and 1100 km s^{-1} expansion velocity are consistent with an explosion date around 1181 CE. The remnant's unusual appearance may be due to the photoionization of wind-driven ejecta due to clump-wind interactions caused by the central star's high-luminosity wind.

Keywords: SN: individual objects: ISM: supernova remnants

1. INTRODUCTION

For nearly 50 years, the young Galactic supernova remnant (SNR) 3C 58 has been viewed as the likely remnant associated with the historical guest star reported by Chinese and Japanese astronomers in early August of 1181 CE, which had a peak brightness ~ 0 mag and was visible for about six months (Stephenson 1971; Clark & Stephenson 1978; Stephenson & Green 2002). The location of 3C 58 in Cassiopeia is close to the reported position of the 1181 guest star, and this along with its $\simeq 10^3 \text{ km s}^{-1}$ expansion velocity (Fesen et al. 2008), its young 65.7 ms pulsar (PSR J0205+6449) (Murray et al. 2002; Camilo et al. 2002) plus the lack of any other young SNR known near the guest star's reported location made it the presumptive SN 1181 remnant.

However, this SN – SNR link was not without problems (Kothes 2013, 2017). Given 3C 58's apparent angular size, proper motion measurements using optical and radio images spanning one or more decades showed positional shifts far less than expected if 3C 58 were associated with the historic guest star of 1181 CE (van den Bergh 1990; Bietenholz 2006; Fesen et al. 2008). Moreover, X-ray studies set strong upper limits on the thermal emission from the surface of 3C 58's 66 ms pulsar which fall well below predictions of standard neutron star cooling, thereby requiring an exotic neutron star cooling processes if linked to SN 1181 and thus only ~ 850 yr old.

A newly recognized Galactic nebula, Pa 30 (G123.1+4.6), located not far from 3C 58 and actually nearer the spot cited by Chinese and Japanese observers, has recently been identified as the likely true remnant of SN 1181 (Ritter et al. 2021; Lykou et al. 2022; Schaefer 2023). Initially identified as a possible planetary nebula (Patchick candidate number 30), it was subsequently found associated with a very hot star ($\sim 210,000 \text{ K}$) with an astounding $16,000 \text{ km s}^{-1}$ velocity wind (Gvaramadze et al. 2019; Garnavich et al. 2020). A young SNR with a hot surviving compact object suggests that it may be the remnant of a double-degenerate merger leading to a subtype Ia SN known as a SN Iax (Gvaramadze et al. 2019; Kashiya et al. 2019; Oskinova et al. 2020; Ritter et al. 2021; Lykou et al. 2022).

The Pa 30 remnant is bright in the mid-infrared (Gvaramadze et al. 2019; Ritter et al. 2021) and has been detected in X-rays (Oskinova et al. 2020). But no associated H α emission has been firmly detected (Gvaramadze et al. 2019; Lykou et al. 2022). Deep [O III] $\lambda 5007$ line emission images revealed a faint and diffuse emission nebula (Kronberger et al. 2014; Ritter et al. 2021) while spectra show [S II] $\lambda\lambda 6716, 6731$ emission with an expansion velocity $\approx 1100 \text{ km s}^{-1}$ (Ritter et al. 2021). Because of its known [S II] emission and a high estimated interstellar extinction ($E(B - V) \simeq 0.88$; Ritter et al. 2021; Lykou et al. 2022), we thought it worthwhile

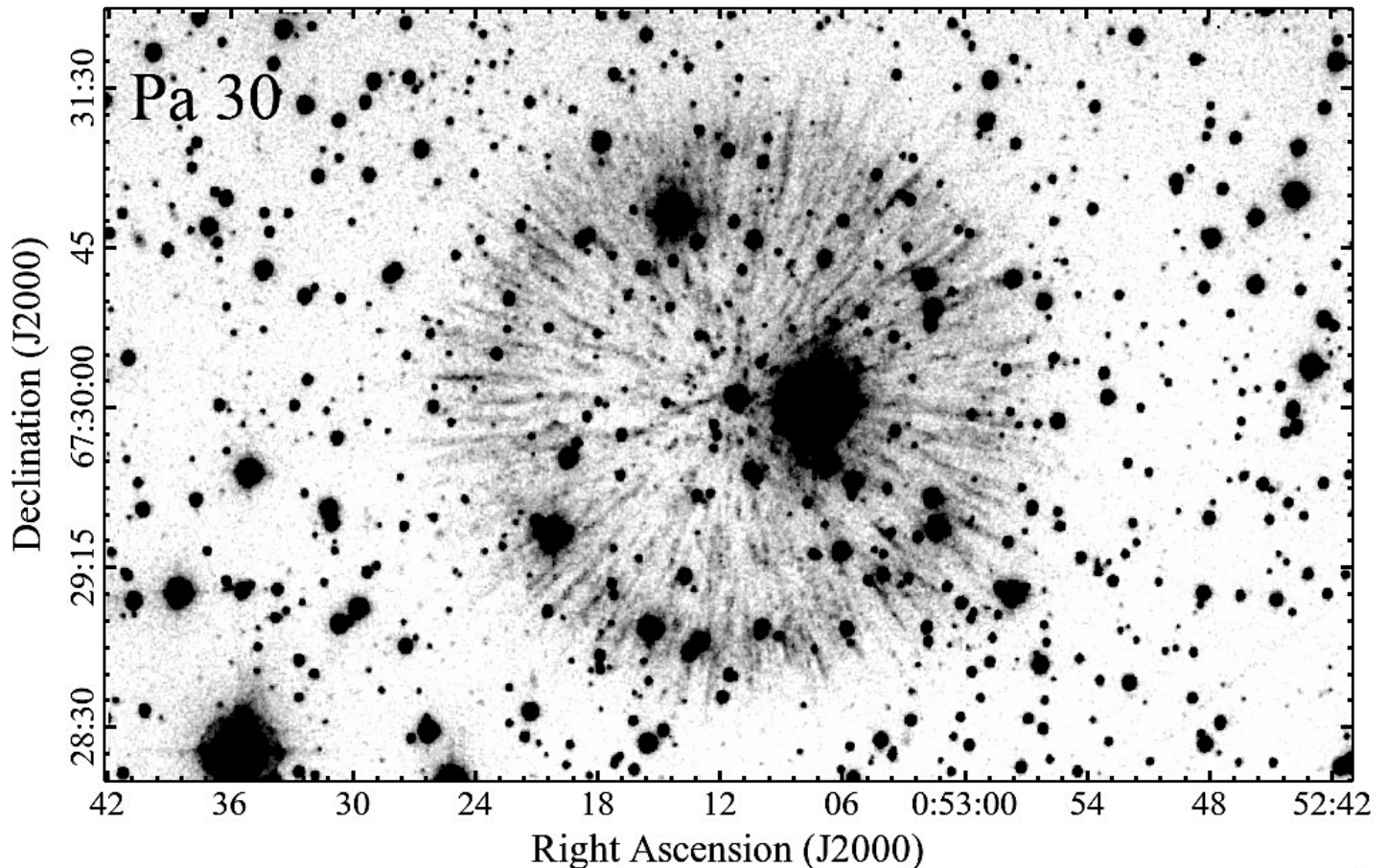


Figure 1. A [S II] $\lambda\lambda 6716, 6731$ image of Pa 30 revealing a highly filamentary and radial morphology.

to explore the optical structure of this young and nearby suspected SN Iax remnant through red [S II] images.

2. OBSERVATIONS

Narrow passband images and low-dispersion spectra of Pa 30 were obtained on 25 and 26 October 2022 with the Hiltner 2.4 m telescope at the MDM Observatory at Kitt Peak, Arizona using the Ohio State Multi-Object Spectrograph (OSMOS; [Martini et al. 2011](#)). This instrument employs a 4096×4096 CCD for both imaging and spectra. In imaging mode, this telescope/camera system yields a clear FOV of $18' \times 18'$. On-chip 2×2 pixel binning gave a spatial resolution scale of $0.55''$ per pixel. Both nights were photometric, with seeing varying from $0.9''$ to $1.3''$.

Three 2000s exposures were taken of the Pa 30 remnant using a 63 \AA FWHM [S II] $\lambda\lambda 6716, 6731$ filter with a T_{max} of 88% centered at $\lambda 6723$. No equally deep off-band images were taken. The [S II] images were bias subtracted, flat-field corrected, and median filter combined. FK5 WCS coordinates were applied with rms errors less than $0.15''$ in both RA and Dec.

Two low-dispersion spectra of the remnant's filaments employing a red VPH grism ($R = 1600$) and a $15'$ long

$1.4''$ wide N-S slit were taken centered on the central star and $\simeq 45''$ west of it. Single exposures of 4000s and 4500 s were taken covering the wavelength $4000\text{--}8900 \text{ \AA}$ with a spectral scale of $3.02 \text{ \AA pixel}^{-1}$ and a FWHM of 7.8 \AA . Although spectral coverage was nearly 5000 \AA , the camera and grism system was most sensitive in the $6000\text{--}7500 \text{ \AA}$ region. Wavelength calibrations were made through Hg-Ne and Ar comparison lamp spectra. Radial velocity measurements are thought accurate to $\pm 30 \text{ km s}^{-1}$ and $\pm 50 \text{ km s}^{-1}$ for bright and faint emission features, respectively.

3. RESULTS

Figure 1 presents our [S II] image of Pa 30 which reveals an unexpectedly filamentary remnant unlike any other Galactic SNR. The remnant is composed of dozens of long, narrow and radially aligned filaments with typical lengths between $5''$ and $20''$ ($0.06\text{--}0.24 \text{ pc}$ at $d = 2.4 \text{ kpc}$) with length/width ratios $\simeq 5\text{--}10$ given the $\simeq 1''$ image resolution. Unlike Pa 30's diffuse appearance reported via its faint detection in [O III] $\lambda 5007$ emission ([Kronberger et al. 2014](#); [Ritter et al. 2021](#)), there is little diffuse emission seen in our [S II] image.

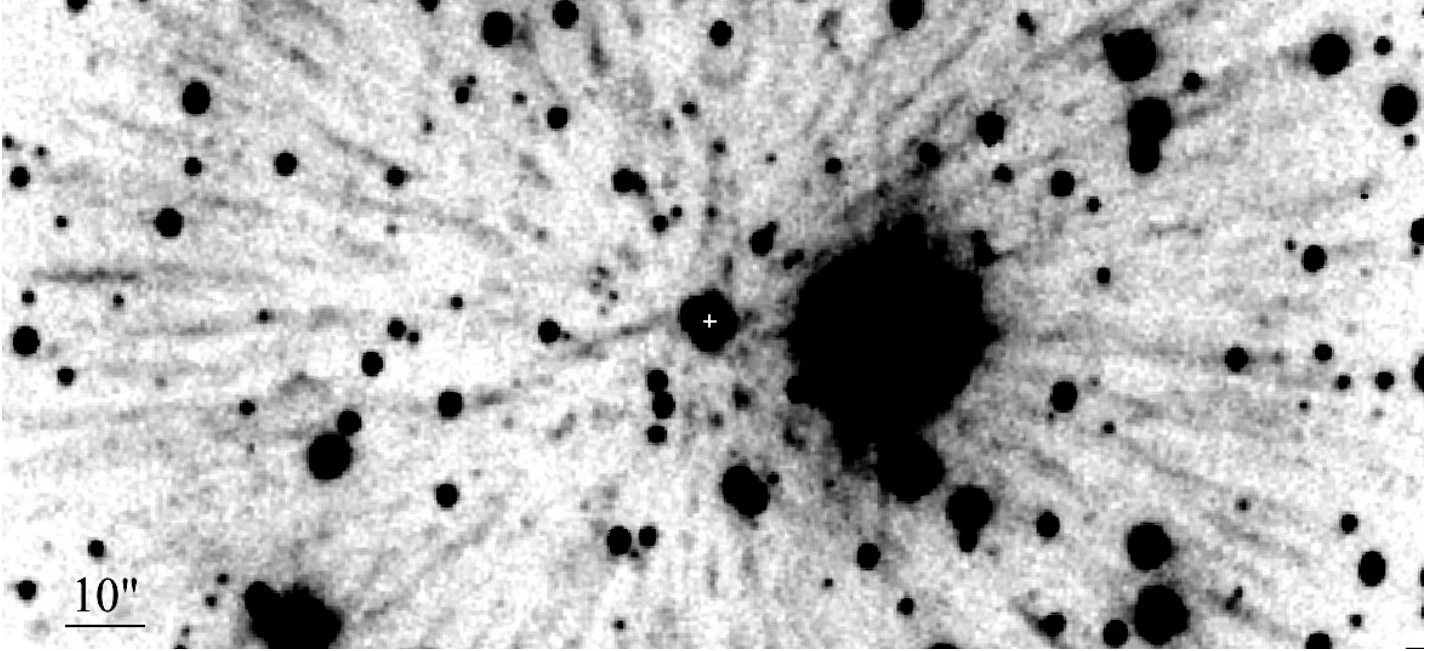


Figure 2. Blowup of Pa 30’s central region. A white cross marks the central star, J005311. North is up, East to the left.

The remnant exhibits a very high degree of circular symmetry with a radii of $85''$ and $90''$ encompassing $>95\%$ and $>98\%$ respectively of the nebula’s [S II] emission. Instead of a sharp and well defined remnant boundary, its outermost filaments fade rapidly with increasing radial distance past $r \simeq 85''$. While the nebula’s filaments are relatively uniform in brightness and length as a function of azimuth angle, one or two contain small knots. Comparison with PanSTARRS r-band images, some stellar-like features near the remnant’s center are actually small knot-like emission features.

The remnant’s hot central star, called J005311 based on its J2000 coordinates ($\alpha=00^{\text{h}}53^{\text{m}}11.2^{\text{s}}$, $\delta=+67^{\circ}30'2.4''$), has been proposed to be either a high mass white dwarf (WD), a super-Chandrasekhar-mass WD, or the result of a double degenerate merger which resulted in a SN Iax explosion (Gvaramadze et al. 2019; Kashiyama et al. 2019; Oskinova et al. 2020; Lykou et al. 2022). While the convergence point of the remnant’s filaments lies very close to Pa 30’s hot central star, some filaments do not appear in perfect alignment with the star’s current position.

This can be seen in Fig. 2 which presents an enlargement of the central region of our [S II] image. The remnant’s hot central star is marked here by a white cross. A relatively bright $12''$ long filament located nearly due east of the central star near the left-hand edge of Fig. 2 is an example of such an apparent mis-alignment, where the filament appears to point back to a position a bit

north of the central star current location¹. However, a statistical analysis of an unbiased selection of nearly 100 filaments show a large convergence scatter of some $\pm 7''$. This large scatter is likely due to both the image’s limited angular resolution and low S/N of many of the remnant’s filaments, plus possible confusion caused by overlapping filaments and knots. Consequently, while it is clear that the hot star lies near the center of the [S II] nebula, we cannot presently determine whether or not if the star’s current position is the exact focal point of Pa 30’s optical filaments.

Figure 3 shows the precise slit locations along with 2D sky background subtracted spectra for the small spectral region around the [S II] doublet for our center and west slit positions. Line emissions from several filaments and knots are readily seen in both slit spectra. The left-right, right-left tilting of the respective red and blueshifted [S II] $\lambda\lambda 6716, 6731$ lines above and below the spectrum of the center star seen in the center slit spectrum is due to viewing extended emission filaments possessing a velocity dispersion along its length where the velocity increases with distance from the expansion center.

Detected [S II] emissions in the center slit data are shown more clearly in Fig. 4. Blueshifted radial velocities ranging from -900 to -960 km s^{-1} and redshifted velocities from $+750$ to $+880 \text{ km s}^{-1}$ are seen close to Pa 30’s central star. No low or intermediate velocity emission features ($v_r \leq 700 \text{ km s}^{-1}$) near the center of

¹ The star’s Gaia EDR3 estimated proper motion in declination is $-0.988 \text{ mas yr}^{-1}$ meaning a shift of less than $1''$ in 1000 yr.

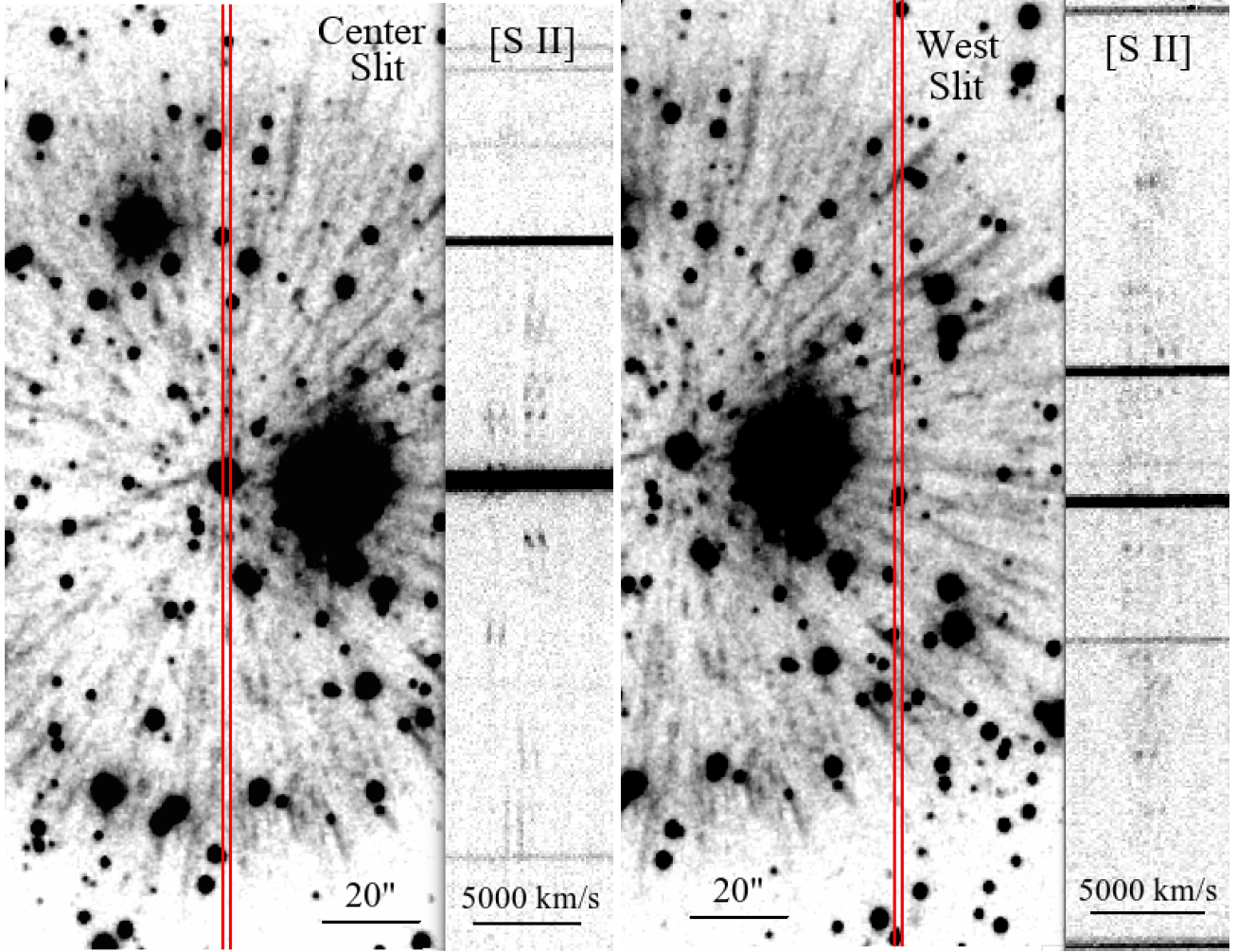


Figure 3. Pair of [S II] $\lambda\lambda 6716,6731$ images of Pa 30 showing central (left) and west (right) slit positions along with the resulting 2D spectra covering the region around the [S II] emission doublet with wavelength increasing from left to right. Ordinary background stars have their continuum spectra visible as horizontal black lines, with the saturated spectrum of Pa 30’s central star, J005311, appearing as an especially wide horizontal black line in the center slit spectrum.

the remnant were detected suggesting a shell-like emission structure.

The bright redshifted knot south of the center star with a radial velocity of $+800 \text{ km s}^{-1}$ exhibited a higher velocity ‘tail’ extending to $+990 \pm 50 \text{ km s}^{-1}$. A blueshifted emission feature just below and nearly hidden by the central star showed a velocity dispersion of -900 to -1130 km s^{-1} . The highest velocity of this nearly dead center emission feature plus a radial velocity of $+1060 \pm 50 \text{ km s}^{-1}$ for a faint knot $20''$ north of Pa 30’s center star suggests a maximum expansion velocity for the nebula of $\simeq 1100 \text{ km s}^{-1}$, consistent with that reported by Ritter et al. (2021).

Although fainter, the spectrum obtained in the western portion of Pa 30 looks quite different. It shows knots with a fairly constant red and blue shifts ($v = \pm 650 \pm 100 \text{ km s}^{-1}$) along most of the slit’s length un-

til near the north and south ends where the expansion velocities drop below $\sim 300 \text{ km s}^{-1}$.

The electron density sensitive [S II] $\lambda 6716/\lambda 6731$ line ratio was measured for the brightest filaments and found to range between 1.5 to 0.9 indicating electron densities between $\leq 100 \text{ cm}^{-3}$ to $\sim 700 \text{ cm}^{-3}$ with an average ratio of around 1.3 implying an electron density $\sim 200 \text{ cm}^{-3}$ (Osterbrock & Ferland 2006). For example, for the four knot spectra plotted in the right panel of Fig. 4, we measure (moving from north to south) $I(\lambda 6716)/I(\lambda 6731)$ values of 1.1, 1.5, 1.3, and 1.3 indicating electron densities ranging from $\leq 100 \text{ cm}^{-3}$ to $\simeq 300 \text{ cm}^{-3}$.

Although Ritter et al. (2021) do not quote electron densities measured from their GTC/OSIRIS observed [S II] line ratios, Lykou et al. (2022) states the average [S II] derived density value from those data was 120 cm^{-3} , which is a bit lower than the average we

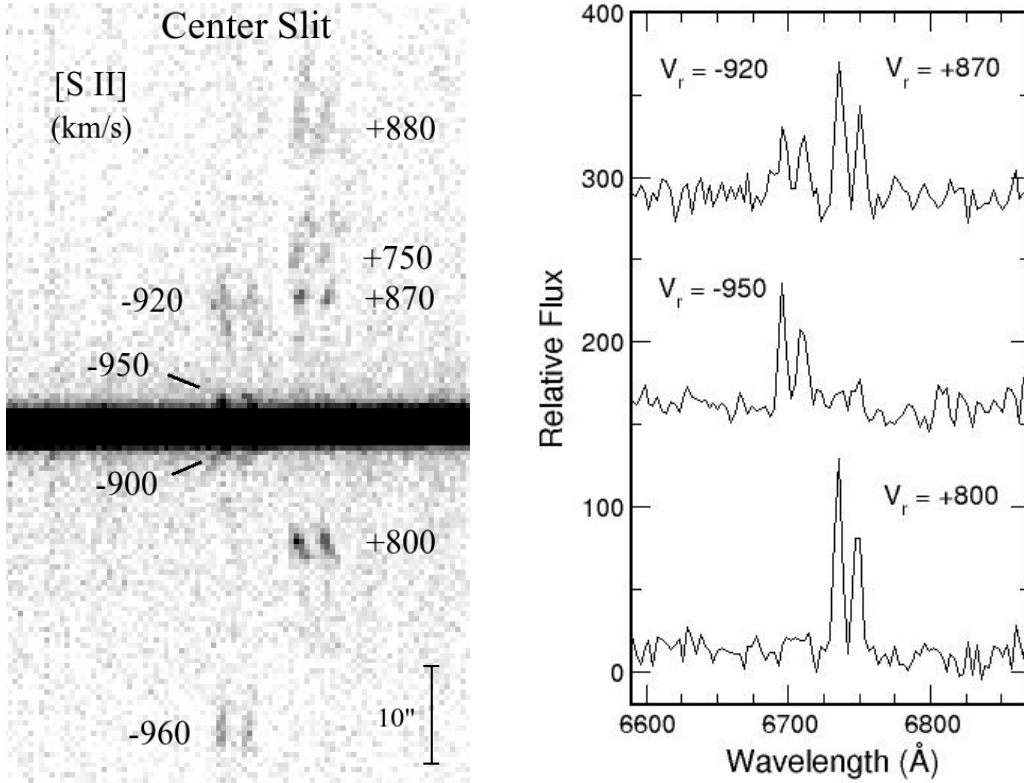


Figure 4. *Left:* Blowup of the middle region of the center slit spectrum showing [S II] $\lambda\lambda 6716, 6731$ emissions along with measured radial velocities. Wavelength increases from left to right. *Right:* Spectra for four of the brightest emission knots detected in the center slit covering the [S II] doublet lines.

found. Also, in the few cases where there was a significant brightness difference between the ends of a filament, the filaments' brightest portion displayed the lowest velocity, suggesting the densest portions of these filaments lies closer in to the remnant's center.

Besides [S II] line emission, very weak [Ar III] $\lambda 7136$ emission was also detected but only near the location of the brightest [S II] emitting knots. No clumpy $H\alpha$ emission was detected at any point along either slit extending at least two arcminutes north and south from Pa 30's central star ($\lambda 6716/H\alpha > 5$), and no other strong, clumpy line emissions were seen within the 6000–8000 Å wavelength range including [N II] $\lambda\lambda 6548, 6583$ and [O II] $\lambda\lambda 7319, 7330$ suggesting a S, Ar rich but H poor emission remnant. However, Lykou et al. (2022) claim the possible detection of faint $H\alpha$ emission from an “outer Pa 30 nebula” based upon a single enhanced pixel at Pa 30's position in the Virginia Tech Spectral-line Survey (VTSS; Dennison et al. 1998).

Finally, in the remnant's eastern half, the majority of emission lies within a projected shell of thickness $\sim 45''$ starting at an inner radius of $35'' \pm 10''$. This may not be true for the remnant's western half where the saturated image of an unrelated bright star prevents an accurate assessment. We note that a shell-like structure would

be similar in size and shape to the shell-like morphology seen in the WISE 22 μm image (see Fig. 5).

4. DISCUSSION

Our image and spectral data show Pa 30 to possess a unique and unexpected optical nebula, one quite unlike any other Galactic supernova remnant (SNR). Instead of the diffuse remnant reportedly seen in a series of 1200 s [O III] exposures taken in 2013 by G. Jacoby using the KPNO 2.1m (Kronberger et al. 2014; Ritter et al. 2021), when viewed in [S II] emission Pa 30 displays a nebula consisting of dozens of radial aligned filaments pointing back to the center of the nebula.

Why Pa 30 is so different from other young Galactic SNRs may be due in part to the presence of its highly luminous and unusual central star which has a spectrum similar to O-rich WO type Wolf-Rayet stars but with no helium emission. Its O VI line widths indicate an exceptional wind velocity of $16,000 \pm 1000 \text{ km s}^{-1}$, some three fold higher than seen in any WO type star (Gvaramadze et al. 2019; Garnavich et al. 2020).

This high speed wind is not thought to be driven by radiation pressure but rather through magnetic torque and pressure gradient from the star's strong magnetic field ($\sim 10^6\text{--}8 \text{ G}$) and fast spin (Gvaramadze et al. 2019; Kashiyama et al. 2019; Lykou et al. 2022). The star

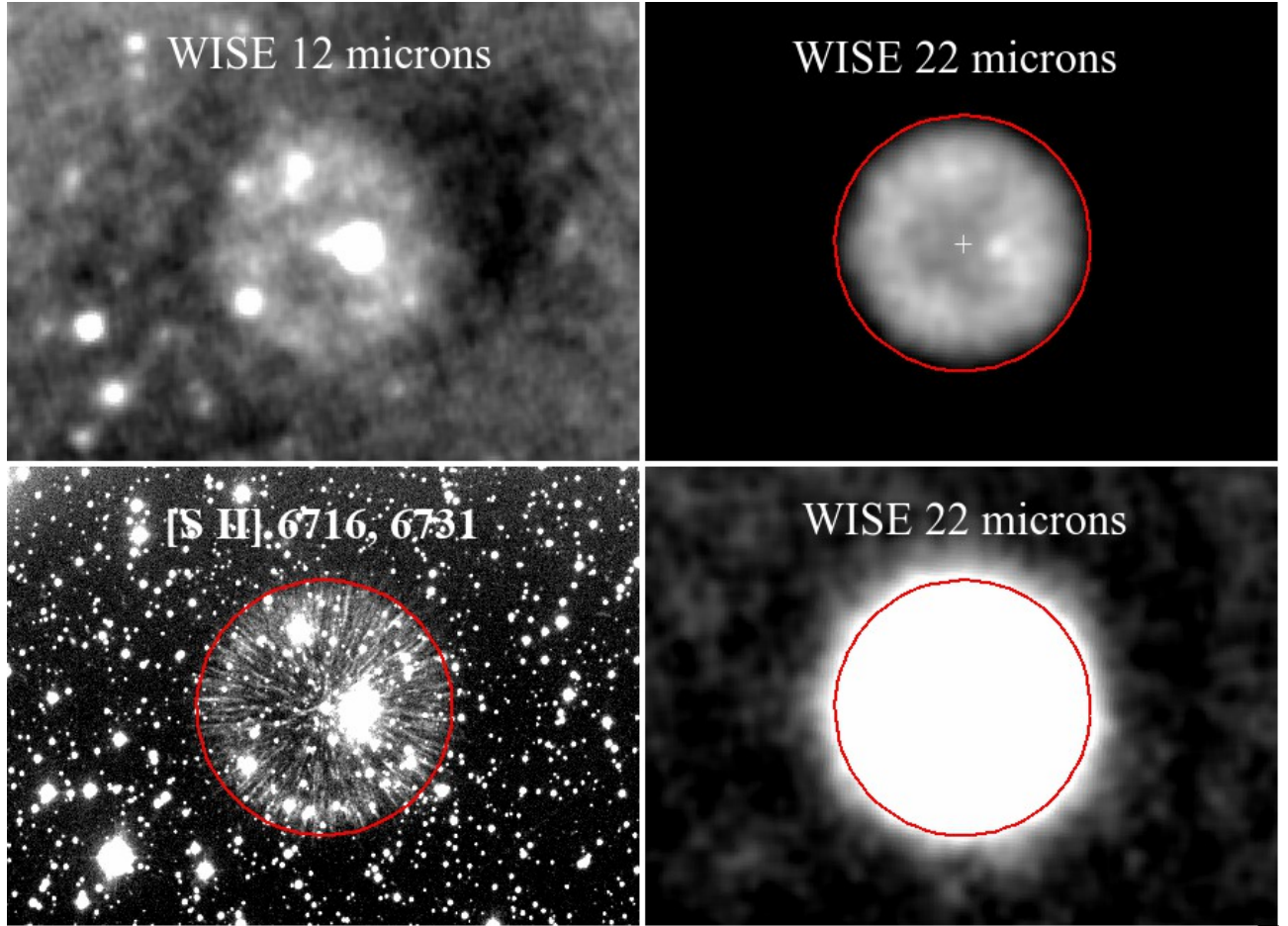


Figure 5. Comparison of WISE 11 μm and 22 μm images with our [S II] image of Pa 30. Red circles are $85''$ in radius and centered on the hot star, J005311, whose position is marked by a white cross in the upper right panel. North is up, East to the left.

also has a high estimated temperature around 210,000 K, a mass loss rate of $3.5 \times 10^{-6} M_{\odot} \text{ yr}^{-1}$ and a $\log(L/L_{\odot}) = 4.6$ (Gvaramadze et al. 2019; Lykou et al. 2022). Consequently, the Pa 30 SNR is different from most SNRs in that the ejecta we see may not be shock heated but rather photoionized by its central star.

Because of its unusual central star, Pa 30 has been suggested as being a SNR arising from a double-degenerate merger leading to a type Ia supernova known as a SN Iax event (Gvaramadze et al. 2019; Kashiyama et al. 2019; Oskina et al. 2020; Ritter et al. 2021; Lykou et al. 2022). SN Iax are characterized as subluminous SNe, the faintest of which have $M_{V, \text{peak}} = -13$ to -16 (Srivastav et al. 2022), show unusually low expansion velocities near maximum ($2000 - 7000 \text{ km s}^{-1}$; Foley et al. 2013; Jha 2017) and some may leave a luminous stellar remnant (e.g., SN 2008ha; Foley et al. 2014, SN 2012Z; McCully et al. 2022). Some SN Iax such as SN 2002cx, the prototype of the subtype, also show unusually low emission line velocities at late times (700 km s^{-1} ; Jha et al. 2006). However, Pa 30's highly spherical mor-

phology is in sharp contrast to the strongly asymmetric SN Iax ejecta in some models (Kashyap et al. 2018).

4.1. The Expansion Velocity of Pa 30

Despite its explosive appearance, Pa 30 displays an unusually low expansion velocity compared to that commonly seen in SNe or young SNRs. Based on its optical [S II] line emissions, Pa 30 has an expansion velocity of $\sim 1100 \text{ km s}^{-1}$ from both on GTC/OSIRIS spectra (Ritter et al. 2021) and in our spectral data. What is unclear, however, is whether the velocity of its [S II] filaments might have been decelerated or essentially undecelerated due to its expansion into a very low density medium around the SN progenitor system.

The timescale for an ejecta knot deceleration (drag) is given by $\tau_{\text{drag}} \sim \chi R_k / V_k$ where χ is the density contrast between the knot and the ambient medium (i.e., ρ_k / ρ_a), R_k is the ejecta knot radius, and V_k is the knot's velocity which in this case would be 1100 km s^{-1} (Jones et al. 1994). Because of the unresolved appearance of the handful of clumps in Pa 30's filaments, the dimensions of possible ejecta knots are presently unknown. Choos-

ing an angular size of $0.1''$ corresponds to $\sim 4 \times 10^{10}$ km at a distance of 2.4 kpc. Adopting a low ambient density of the binary WD system prior to SN outburst of 0.01 cm^{-3} hence a $\chi \sim 3 \times 10^4$ based on our average electron density of 300 cm^{-3} , leads to a $\tau_{\text{drag}} \sim 3 \times 10^4$ yr, suggesting little appreciable deceleration in 1000 yr. However, much smaller ejecta fragments will decelerate more rapidly owing to their larger surface area-to-mass ratios.

4.2. The Nature of Pa 30's Long Emission Filaments

The morphology of Pa 30's filamentary nebulosity does not have close analogues in the remnants of either young Galactic SNe or novae. Faint trailing ablated material ($\sim 10^{16}$ cm) has been seen for 8,000 – 12,000 km s^{-1} SN ejecta in the young SNR Cassiopeia A (Fesen et al. 2011). Comet-like structures with lengths up to $\sim 10^{17}$ cm off the 600 – 1000 km s^{-1} nova ejecta clumps seen in the case of GK Per (Nova Per 1901) has been interpreted as either ejecta running into a pre-existing ambient medium (Shara et al. 2012) or ablation from clump-wind interactions with dwarf nova wind velocities of several thousand km s^{-1} (Harvey et al. 2015). Possible analogues to Pa 30's filaments might be the ablated wind blown tails seen in nova DQ Her (Vaytet et al. 2007) which have terminal velocities of 800-900 km s^{-1} .

Cometary tails have also been seen in some planetary nebulae, such as the Helix Nebula (O'Dell & Handron 1996; Meaburn et al. 1998) which have been attributed to a moderately supersonic stream or wind of photoionized gas overrunning a slower expanding mass partially evaporated by photoionization which is then accelerated by momentum transfer (Dyson et al. 2006; Matsuura et al. 2009). Shadows behind dense clumps immersed in a photoionized medium has also been proposed to explain thin, luminous filaments seen in some PNe (van Blerkom & Arny 1972; Cantó et al. 1998; Raga et al. 2009). Long and wide tails have also been seen in bow shocks “fingers” behind high-velocity clumps such as in the BN/KL Orion OMC1 outflow (Bally et al. 2015).

In all these examples there is an identifiable knot or clump undergoing the visible mass loss. But few if any of Pa 30's [S II] filaments show evidence of an emission clump or knot at either the start or end of the filaments in our image (cf. Figs. 1 & 2). Instead, most filaments show little brightness variation along the majority of their $\sim 5 \times 10^{17}$ cm lengths. In addition, the electron density of the Pa 30's filaments is a modest $100\text{--}300 \text{ cm}^{-3}$, low for SN ejecta which is typically $10^3\text{--}4 \text{ cm}^{-3}$.

Nonetheless, we view it likely that Pa 30's unusual morphology may be related to the stellar winds of its central star, an object unlike anything in any other nova or young Galactic SNR. Hydrodynamic models show that supersonic flows produce short tails, while subsonic ones form long tails (Pittard et al. 2005; Dyson et al. 2006). This suggests that Pa 30's long filaments are the result of subsonic or mildly supersonic wind off

its central star that is accelerating some of the lower density SN ejecta. In such a scenario, an expanding cloud of partially clumpy SN ejecta is sculptured into filaments by Rayleigh-Taylor instabilities through interaction with the central star's stellar winds, then made visible by photoionization by the central star.

Our center slit spectrum supports this picture by showing that some of the [S II] emission filaments possess a dispersion of velocities of order a few hundred km s^{-1} . In addition, the extended emission lines seen in the filament's red and blue shifted velocity dispersion is consistent with the velocity of a filament's emission increasing along its length with increasing distance from the remnant's center much like that seen in clump-wind interactions in novae (DQ Her; Vaytet et al. 2007).

Moreover, Oskinova et al. (2020) has suggested that the ‘hole’ seen in the WISE 22 μm image (see top right panel in Fig. 4) is due to the snowplow effect of Pa 30's central star's wind luminosity. A hole in the remnant's expansion structure would help explain the lack of low and intermediate velocity ejecta (i.e., $v_r \leq 600 \text{ km s}^{-1}$) seen in our center and west slit position spectra (Figs. 3 and 4). Furthermore, in the SN Iax merger models of Shen & Schwab (2017), the stellar winds off the bound merger WD may have been considerably stronger in the past, especially during the first one or two decades after outburst.

Although a photoionized clump-wind interaction scenario is highly suggestive, we cannot reach a firm conclusion regarding the nature of the Pa 30 filaments given the limited data in hand. Deeper and higher resolution images taken in [S II] and other emission lines including higher-ionization lines could help clarify the nature of these filaments and the possible presence of filament knots. Higher resolution images may also help determine the nebula's precise convergence point which could then address the possibility of a WD merger star kick as suggested in some SN Iax models (Kashyap et al. 2018; Lach et al. 2022).

4.3. Pa 30 as the Remnant of SN 1181 CE

There is now considerable circumstantial evidence linking the Pa 30 SNR to the historical guest star of 1181 CE which might have been a subluminal SN Iax event. Pa 30 lies in a region of the sky close to the recorded position of the historical guest star (Ritter et al. 2021; Schaefer 2023) and its expansion velocity suggests an age consistent with the late 12th century supernova of 1181 CE.

Using estimates of the remnant's energy and the local ISM density, Oskinova et al. (2020) suggested an age of 300-1100 yr. Adopting a remnant radius of $100''$ based on the remnant's 22 μm WISE data, a distance of 2.3 ± 0.14 kpc based on Gaia EDR3 parallax values (Lykou et al. 2022) and an undecelerated expansion velocity of $\simeq 1100 \text{ km s}^{-1}$ based on GTC/OSIRIS [S II]

line emission, Ritter et al. (2021) estimated an age of 990^{+280}_{-220} yr.

However, using an angular radius of $85''$ more representative of the remnant's [S II] filaments (see Fig. 5) yields a current age for Pa 30 of 844 ± 55 yr. This is in excellent agreement with the current 841 yr age of SN 1181. Adopting instead a 2.4 kpc distance (Schaefer 2023) changes this to 882 ± 58 yr, still a very good match. These estimates are valid even if the nebula's filamentary emission seen has been wind accelerated as long as the measured ejecta expansion velocity reflects any wind-driven acceleration. Consequently, this strongly suggests, but does not prove, that Pa 30 is the remnant of SN 1181 CE.

Finally, the peak visual magnitude of SN 1181 has been estimated to be between +1.0 and -0.5 (Ritter et al. 2021) or 0.0 and -1.4 (Schaefer 2023) which, assuming an $A_V \sim 2.4$ -2.9 mag (Ritter et al. 2021; Lykou et al. 2022), implies M_V values between -12 and -16. Such numbers indicate a subluminal SN event, consistent with the picture of a SN 1181 being a subluminal type Ia event which shows similar values (Jha 2017; Srivastav et al. 2022). The presence of a hot central stellar remnant completes the picture of Pa 30 as a young SNR from a double-degenerate merger in a SN Ia event as some have proposed (Kashiyama et al. 2019; Oskinova et al. 2020).

5. CONCLUSIONS

Our deep [S II] $\lambda\lambda 6716, 6731$ images and optical low-dispersion spectra of Pa 30 reveal:

- 1) A highly structured, radially aligned filamentary nebula with a convergence point near its hot and peculiar central star.
- 2) A peak expansion velocity $\simeq 1100$ km s $^{-1}$, a complete lack of low or intermediate velocity filaments, electron densities of ≤ 100 to 700 cm $^{-3}$, and a thick shell-like

structure resembling its appearance in 22 μ m WISE images.

3) No H α emission was detected from the nebula ([S II] $\lambda 6716/\text{H}\alpha > 5$), with the only other line emission detected being very faint [Ar III] $\lambda 7136$ suggesting a S, Ar-rich but H-poor remnant.

4) The remnant's unusual appearance may be due to the photoionization of wind blown ejecta clump-wind interaction due to the central star's high-luminosity winds.

5) Consistent with the conclusions of Ritter et al. (2021), Lykou et al. (2022) and Schaefer (2023), we find that Pa 30 is the likely remnant of the Galactic SN sighted in 1181 CE.

Higher resolution, multi-wavelength optical and infrared images should help clarify this young remnant's structure, the convergence point of its filaments, and the role of the nebula's central star may have played in the formation of its filaments and central IR cavity. Pa 30's relatively small distance, its interesting and complex optical and infrared structures centered on a highly unusual star, plus a precisely known age if linked to the supernova event of 1181 CE, all combine to make it an important nebulosity for further study.

We thank the anonymous referee, Bruce Balick, Roger Chevalier, George Jacoby, Dan Milisavljevic, Dan Patnaude, and Noam Soker for helpful comments and suggestions. We also thank Eric Galayda and the MDM staff for making these observations possible so soon after the June 2022 fire on Kitt Peak mountain. This work is part of R.A.F.'s Archangel III Research Program at Dartmouth. We have made use of the Simbad database, NASA's Skyview online data archives, and data from the European Space Agency mission Gaia (<https://www.cosmos.esa.int/gaia>), processed by the Gaia Data Processing and Analysis Consortium (DPAC, <https://www.cosmos.esa.int/web/gaia/dpac/consortium>).

Facilities: MDM Observatory (OSMOS)

Software: PYRAF Green (2012), XMGrace

REFERENCES

- Bally, J., Ginsburg, A., Silvia, D., & Youngblood, A. 2015, A&A, 579, A130, doi: [10.1051/0004-6361/201425073](https://doi.org/10.1051/0004-6361/201425073)
- Bietenholz, M. F. 2006, ApJ, 645, 1180, doi: [10.1086/504584](https://doi.org/10.1086/504584)
- Camilo, F., Stairs, I. H., Lorimer, D. R., et al. 2002, ApJL, 571, L41, doi: [10.1086/341178](https://doi.org/10.1086/341178)
- Cantó, J., Raga, A., Steffen, W., & Shapiro, P. R. 1998, ApJ, 502, 695, doi: [10.1086/305946](https://doi.org/10.1086/305946)
- Clark, D. H., & Stephenson, F. R. 1978, Astrophys. Lett., 19, 142
- Dennison, B., Simonetti, J. H., & Topasna, G. A. 1998, PASA, 15, 147, doi: [10.1071/AS98147](https://doi.org/10.1071/AS98147)
- Dyson, J. E., Pittard, J. M., Meaburn, J., & Falle, S. A. E. G. 2006, A&A, 457, 561, doi: [10.1051/0004-6361:20065550](https://doi.org/10.1051/0004-6361:20065550)
- Fesen, R., Rudie, G., Hurford, A., & Soto, A. 2008, ApJS, 174, 379, doi: [10.1086/522781](https://doi.org/10.1086/522781)
- Fesen, R. A., Zastrow, J. A., Hammell, M. C., Shull, J. M., & Silvia, D. W. 2011, ApJ, 736, 109, doi: [10.1088/0004-637X/736/2/109](https://doi.org/10.1088/0004-637X/736/2/109)
- Foley, R. J., McCully, C., Jha, S. W., et al. 2014, ApJ, 792, 29, doi: [10.1088/0004-637X/792/1/29](https://doi.org/10.1088/0004-637X/792/1/29)

- Foley, R. J., Challis, P. J., Chornock, R., et al. 2013, *ApJ*, 767, 57, doi: [10.1088/0004-637X/767/1/57](https://doi.org/10.1088/0004-637X/767/1/57)
- Garnavich, P., Littlefield, C., Pogge, R., & Wood, C. 2020, *Research Notes of the American Astronomical Society*, 4, 167, doi: [10.3847/2515-5172/abbb8b](https://doi.org/10.3847/2515-5172/abbb8b)
- Green, W. 2012, *Society for Astronomical Sciences Annual Symposium*, 31, 159
- Gvaramadze, V. V., Gräfener, G., Langer, N., et al. 2019, *Nature*, 569, 684, doi: [10.1038/s41586-019-1216-1](https://doi.org/10.1038/s41586-019-1216-1)
- Harvey, E., Redman, M. P., Boumis, P., & Akas, S. 2015, in *EAS Publications Series*, Vol. 71-72, *EAS Publications Series*, 95–99, doi: [10.1051/eas/1571018](https://doi.org/10.1051/eas/1571018)
- Jha, S., Branch, D., Chornock, R., et al. 2006, *AJ*, 132, 189, doi: [10.1086/504599](https://doi.org/10.1086/504599)
- Jha, S. W. 2017, in *Handbook of Supernovae*, ed. A. W. Alsabti & P. Murdin, 375, doi: [10.1007/978-3-319-21846-5_42](https://doi.org/10.1007/978-3-319-21846-5_42)
- Jones, T. W., Kang, H., & Tregillis, I. L. 1994, *ApJ*, 432, 194, doi: [10.1086/174560](https://doi.org/10.1086/174560)
- Kashiyama, K., Fujisawa, K., & Shigeyama, T. 2019, *ApJ*, 887, 39, doi: [10.3847/1538-4357/ab4e97](https://doi.org/10.3847/1538-4357/ab4e97)
- Kashyap, R., Haque, T., Lorén-Aguilar, P., García-Berro, E., & Fisher, R. 2018, *ApJ*, 869, 140, doi: [10.3847/1538-4357/aaedb7](https://doi.org/10.3847/1538-4357/aaedb7)
- Kothes, R. 2013, *A&A*, 560, A18, doi: [10.1051/0004-6361/201219839](https://doi.org/10.1051/0004-6361/201219839)
- . 2017, in *Handbook of Supernovae*, ed. A. W. Alsabti & P. Murdin, 97, doi: [10.1007/978-3-319-21846-5_47](https://doi.org/10.1007/978-3-319-21846-5_47)
- Kronberger, M., Jacoby, G. H., Acker, A., et al. 2014, in *Asymmetrical Planetary Nebulae VI Conference*, ed. C. Morisset, G. Delgado-Inglada, & S. Torres-Peimbert, 48
- Lach, F., Callan, F. P., Bubeck, D., et al. 2022, *A&A*, 658, A179, doi: [10.1051/0004-6361/202141453](https://doi.org/10.1051/0004-6361/202141453)
- Lykou, F., Parker, Q. A., Ritter, A., et al. 2022, *arXiv e-prints*, arXiv:2208.03946, <https://arxiv.org/abs/2208.03946>
- Martini, P., Stoll, R., Derwent, M. A., et al. 2011, *PASP*, 123, 187, doi: [10.1086/658357](https://doi.org/10.1086/658357)
- Matsuura, M., Speck, A. K., McHunu, B. M., et al. 2009, *ApJ*, 700, 1067, doi: [10.1088/0004-637X/700/2/1067](https://doi.org/10.1088/0004-637X/700/2/1067)
- McCully, C., Jha, S. W., Scalzo, R. A., et al. 2022, *ApJ*, 925, 138, doi: [10.3847/1538-4357/ac3bbd](https://doi.org/10.3847/1538-4357/ac3bbd)
- Meaburn, J., Clayton, C. A., Bryce, M., et al. 1998, *MNRAS*, 294, 201, doi: [10.1046/j.1365-8711.1998.01152.x](https://doi.org/10.1046/j.1365-8711.1998.01152.x)
- Murray, S. S., Slane, P. O., Seward, F. D., Ransom, S. M., & Gaensler, B. M. 2002, *ApJ*, 568, 226, doi: [10.1086/338766](https://doi.org/10.1086/338766)
- O’Dell, C. R., & Handron, K. D. 1996, *AJ*, 111, 1630, doi: [10.1086/117902](https://doi.org/10.1086/117902)
- Oskinova, L. M., Gvaramadze, V. V., Gräfener, G., Langer, N., & Todt, H. 2020, *A&A*, 644, L8, doi: [10.1051/0004-6361/202039232](https://doi.org/10.1051/0004-6361/202039232)
- Osterbrock, D. E., & Ferland, G. J. 2006, *Astrophysics of gaseous nebulae and active galactic nuclei*
- Pittard, J. M., Dyson, J. E., Falle, S. A. E. G., & Hartquist, T. W. 2005, *MNRAS*, 361, 1077, doi: [10.1111/j.1365-2966.2005.09268.x](https://doi.org/10.1111/j.1365-2966.2005.09268.x)
- Raga, A. C., Henney, W., Vasconcelos, J., et al. 2009, *MNRAS*, 392, 964, doi: [10.1111/j.1365-2966.2008.14097.x](https://doi.org/10.1111/j.1365-2966.2008.14097.x)
- Ritter, A., Parker, Q. A., Lykou, F., et al. 2021, *ApJL*, 918, L33, doi: [10.3847/2041-8213/ac2253](https://doi.org/10.3847/2041-8213/ac2253)
- Schaefer, B. E. 2023, *arXiv e-prints*, arXiv:2301.04807, doi: [10.48550/arXiv.2301.04807](https://doi.org/10.48550/arXiv.2301.04807)
- Shara, M. M., Zurek, D., De Marco, O., et al. 2012, *AJ*, 143, 143, doi: [10.1088/0004-6256/143/6/143](https://doi.org/10.1088/0004-6256/143/6/143)
- Shen, K. J., & Schwab, J. 2017, *ApJ*, 834, 180, doi: [10.3847/1538-4357/834/2/180](https://doi.org/10.3847/1538-4357/834/2/180)
- Srivastav, S., Smartt, S. J., Huber, M. E., et al. 2022, *MNRAS*, 511, 2708, doi: [10.1093/mnras/stac177](https://doi.org/10.1093/mnras/stac177)
- Stephenson, F. R. 1971, *QJRAS*, 12, 10
- Stephenson, F. R., & Green, D. A. 2002, *Historical supernovae and their remnants*, vol 5, Oxford: Clarendon Press, ISBN 0198507666
- van Blerkom, D., & Arny, T. T. 1972, *MNRAS*, 156, 91, doi: [10.1093/mnras/156.1.91](https://doi.org/10.1093/mnras/156.1.91)
- van den Bergh, S. 1990, *ApJ*, 357, 138, doi: [10.1086/168899](https://doi.org/10.1086/168899)
- Vaytet, N. M. H., O’Brien, T. J., & Rushton, A. P. 2007, *MNRAS*, 380, 175, doi: [10.1111/j.1365-2966.2007.12057.x](https://doi.org/10.1111/j.1365-2966.2007.12057.x)